Inorg. Chem. **2003**, *42*, 8371–8376

A New Look at Bonding in Trialuminides: Reinvestigation of $TaAl_3$

Cathie L. Condron and Gordon J. Miller*

Department of Chemistry, Iowa State University, Ames, Iowa 50011

Joel D. Strand, Sergey L. Bud'ko, and Paul C. Canfield

Ames Laboratory and Department of Physics & Astronomy, Iowa State University, Ames, Iowa 50011

Received August 4, 2003

Single crystals of $TaAl_3$ were grown at high temperatures from an Al-rich, binary solution. $TaAl_3$ adopts the $D0_{22}$ structure type, space group *I*4/*mmm* with $a = 3.8412(5)$ Å, $c = 8.5402(17)$ Å, and $Z = 2$. The structure type, which is the preferred structure for all group 5 trialuminides and $TiAl_3$ as well as the high-temperature form of $HfAl_3$, is a binary coloring of the face-centered-cubic (fcc) arrangement. The distribution of Ta atoms creates a three-dimensional network of vertex and edge-sharing square pyramids of Al atoms. Temperature-dependent electrical resistivity and magnetic susceptibility measurements are consistent with $TaAl_3$ being a metallic compound with a relatively low density of states at the Fermi surface. Furthermore, tight-binding electronic structure calculations are utilized to describe the bonding in these compounds and to compare their stability with respect to the alternative fcc-related, e.g., the $D0_{23}$ ($ZrAl_3$-type) and the $L1_2$ ($AuCu_3$-type), structures. A modified Wade's rule argument provides insights into the structural preferences.

Introduction

Trialuminides of transition and rare earth elements have received a lot of industrial interest for high-temperature applications, e.g., in aerospace concerns, because they offer low densities, high melting points, and large elastic moduli.[1] However, applications have been limited because they tend to be brittle, indicative of significant covalent-type bonding within the intermetallic structure. In addition to high-temperature applications, aluminum-rich intermetallics have shown tendencies to form quasicrystalline structures[2] and polar intermetallic characteristics.[3] Polar intermetallics are identified by analysis of electronic structure calculations that often show pseudogaps at the Fermi level in the density-of-states (DOS) curve as well as maximum metal−metal bonding interactions as quantified by overlap populations.[4] With high-temperature applications of the trialuminides in mind coupled with their brittleness, Freeman and co-workers published a series of articles analyzing the structural stability and electronic structure of various trialuminides, in which they concluded that a simple rigid band approximation is adequate to describe the structural stability of the so-called p−d covalent trialuminides.[5]

As part of an ongoing project to explore the properties of rare earth Ta−Al compounds, single crystals of $TaAl_3$ were grown so as to determine the appropriateness of Al as a solvent. This paper reports the synthesis of $TaAl_3$, the redetermination of its crystal structure by single-crystal X-ray diffraction, and an analysis of its physical properties, electronic structure, and chemical bonding from a different viewpoint than found in earlier publications.

* Corresponding author. Phone: (515) 294-6063. Fax: (515) 294-0105. E-mail: gmiller@iastate.edu.

(1) (a) Lipsitt, H. A. In *Properties of Advanced High-Temperature Alloys*; Allen, S. M., Pelloux, R. M., Widmer, R., Eds.; American Society for Metals: Metals Park, OH, 1986; p 157. (b) Kubel, E. J. *Adv. Mater. Proc. Met. Prog.* **1986**, *130*, 43.

(2) (a) Janot, C. *Quasicrystals: A Primer*, 2nd ed.; Oxford University Press: Oxford, 1994. (b) *Quasicrystals: The State of the Art*; Vincenzo, D. P., Steinhardt, P. J., Eds. World Scientific: New York, 1999. (c) *Physical Properties of Quasicrystals*; Stadnik, Z. M., Ed.; Springer: Heidelberg, 1999.

(3) Miller, G. J.; Lee, C.-S.; Choe, W. In *Inorganic Chemistry Highlights*; Meyer, G., Naumann, D., Wesemann, L., Eds.; Wiley-VCH: Weinheim, Germany, 2002; p 21.

(4) Miller,G. J. In *Chemistry, Structure and Bonding of Zintl Phases and Ions*; Kauzlarich, S. M., Ed.; VCH: New York, 1996; p 1.

(5) (a) Xu, J.-H.; Freeman, A. J. *Phys. Rev. B* **1989**, *40*, 11927−11930. (b) Hong, T.; Watson-Yang, T. J.; Freeman, A. J.; Oguchi, T.; Xu, J.-H. *Phys. Rev. B* **1990**, *41*, 12462−12467. (c) Xu, J.-H.; Freeman, A. J. *Phys. Rev. B* **1990**, *41*, 12553−12561. (d) Xu, J.; Freeman, A. J. *J. Mater. Res.* **1991**, *6*, 1188−1199.

10.1021/ic034927m CCC: $25.00
Published on Web 10/29/2003

Table 1. Selected Crystallographic Data for $TaAl_3$

empirical formula	$TaAl_3$
crystal color, habit	silver, plate
crystal system	tetragonal
space group	*I*4/*mmm* (No. 139)
unit cell dimensions (Å)	$a = 3.8437$ (5), $c = 8.5460$ (17)
Z	2
volume (Å^3)	126.26(3)
density (calcd) (mg/m^3)	3.444
linear abs coeff μ (mm^{-1})	22.087
reflections collected	538
reflections observed ($I \geq 2\sigma$)	61
no. of parameters refined	8
data/parameter ratio	7.63
final *R* indices [$I > 2\sigma(I)$]	$R^a = 0.0079$, $R_w{}^a = 0.0178$
R indices (all data)	$R^a = 0.0079$, $R_w{}^a = 0.0178$
goodness of fit on F^2	1.228
mean shift/error	0.000
max shift/error	0.000
residual electron density (e Å^{-3})	0.750 and −0.639
weighting scheme	$w^{-1} = [\sigma^2(F_o) + (0.0471P)^2 + (0.5945P)]$, where $P = [\max(F_o{}^2,0) + 2F_c{}^2/3]$

[a] $R = \sum||F_o| - |F_c||/\sum|F_o|$; $R_w = [\sum w(|F_o| - |F_c|)^2\}/\sum w|F_o|^2\}]^{1/2}$.

Experimental Section

Synthesis. $TaAl_3$ was synthesized from the elements Ta (99.999%; Ames Laboratory) and Al (99.98%; Alfa) using the high-temperature metallic solution growth method.[6] To study the use of aluminum as a flux for reactions involving Ta, numerous compositions ranging from $Ta_{0.01}Al_{0.99}$ to $Ta_{0.10}Al_{0.90}$ were examined. The elements were combined in a 2 mL alumina crucible, which was placed into a fused silica tube, and a second crucible, filled with SiO_2 wool, was placed inverted on top of the first. The fused silica tube was subsequently sealed under 0.2 atm Ar and placed into a box furnace. The mixtures were heated to 1190 °C in 3 h, allowed to dwell at 1190 °C for 2 h, and then cooled to 800 °C over 90 h. The reaction was removed from the furnace at 800 °C, and the excess liquid was decanted. Upon examination, silver platelike crystals $TaAl_3$ were found. Optimal specimens for single-crystal X-ray diffraction experiments were isolated from the composition $Ta_{0.02}Al_{0.98}$.

Crystallographic Studies. Room temperature (ca. 300 K), X-ray diffraction data of a single crystal of $TaAl_3$ were collected using a Bruker SMART Apex CCD diffractometer with Mo Kα radiation ($\lambda = 0.710\,73$ Å) and a detector-to-crystal distance of 5.08 cm. Data were collected in a full sphere and were harvested by collecting three sets of frames with 0.3° scans in ω for an exposure time of 10 s per frame. The range of 2θ extended from 3.0° to 56.0°. Data were corrected for Lorentz and polarization effects through the SAINT program;[7] absorption corrections were based on fitting a function to the empirical transmission surface as sampled by multiple equivalent reflections (program SADABS[7]).

Unit cell parameters were indexed by peaks obtained from 90 frames of reciprocal space images and then refined using all observed diffraction peaks after data integration. Together with systematic absences, the space group *I*4/*mmm* (No. 139) was selected for subsequent structural analysis. The structure solution was obtained by direct methods and refined by full-matrix least-squares refinement of $F_o{}^2$ using the SHELXTL 5.12 package (see Table 1).

Property Measurements. Magnetization measurements were performed in a Quantum Design MPMS-5 SQUID magnetometer ($T = 1.8-350$ K, $H_{max} = 55$ kG). To acquire a reasonable signal-to-noise ratio, several single crystals of $TaAl_3$ were placed on a piece of Mylar tape which was subsequently mounted on a straw. The Mylar tape alone was also measured, and then subtracted from the sample plus Mylar data to account for any background effects the Mylar tape could have caused. The average error associated with the susceptibility measurements is roughly 20−25%. This is higher than usual because $TaAl_3$ produces a very small signal.

Temperature- and field-dependent resistivity measurements were obtained on a single crystal ($1.0 \times 0.2 \times 0.5$ mm^3) using a standard four probe technique. The electrical resistance in zero and applied field was measured using the ACT option of a Quantum Design PPMS-9 instrument ($f = 16$ Hz, $I = 1-3$ mA) for an arbitrary in-plane direction of the current. Error in the resistivity measurements was small. Most of the error resulted from the uncertainty in the crystal dimensions, which was approximately 5% in each direction. Magnetoresistance was measured in a transverse geometry, i.e., magnetic field perpendicular to the current.

Electronic Structure Calculations. Tight-binding linear muffin-tin orbital calculations using the atomic sphere approximation (TB-LMTO-ASA) were performed on $TaAl_3$ using the LMTO47 program[8] to analyze the chemical bonding and provide insights into its observed structure. Exchange and correlation were treated in a local density approximation.[9] All relativistic effects except spin−orbit coupling were taken into account using a scalar relativistic approximation.[10] The basis set consisted of s, p, d, and f functions for Ta ($R_{WS} = 1.64$ Å) and s, p, and d functions for Al ($R_{WS} = 1.46$ Å for Al1; 1.55 Å for Al2). Due to the nearly close-packed arrangement of atoms in this and related structures, no empty spheres were needed to achieve convergence, and the overlap criterion between Wigner−Seitz spheres was set to a maximum of 16%. *k*-space integrations used the tetrahedron method[11] with 150 *k*-points within the first Brillouin zone to calculate the energy densities of states (DOS) and crystal overlap Hamiltonian population (COHP) curves.[12]

Table 2. Atomic Coordinates and Displacement Parameters for $TaAl_3$

atom	x	y	z	occupancy	U_{eq} (Å)
Ta	0	0	1/2	1	0.003 13 (21)
Al1	1/2	1/2	1/2	1	0.005 44 (51)
Al2	0	1/2	1/4	1	0.004 36 (38)

Results and Discussion

Structure. The structure of $TaAl_3$ is a binary coloring of the face-centered-cubic arrangement of atoms, and given the *Strukturbericht* designation $D0_{22}$.[13] This particular binary coloring creates a body-centered tetragonal unit cell with $c/a = 2.22$. Tables 2, 3, and 4 contain, respectively, positional parameters, thermal displacement parameters, and relevant bond distances. Figure 1 illustrates a projection of its crystal

(6) Canfield, P. C.; Fisk, Z. *Philos. Mag. B* **1992**, *65*, 1117−1123.
(7) *XRD Single-Crystal Software*; Bruker Analytical X-ray Systems: Madision, WI, 1999.
(8) (a) Andersen, O. K. *Phys. Rev. B* **1975**, *12*, 3060. (b) Andersen, O. K.; Jepsen, O. *Phys. Rev. Lett.* **1984**, *53*, 2571. (c) Andersen, O. K.; Jepsen, O.; Glötzel, D. In *Highlights of Condensed-Matter Theory*; Bassani, F., Fumi, F., Tosi, M. P., Lambrecht, W. R. L., Eds.; North-Holland: New York, 1985. (d) Andersen, O. K. *Phys. Rev. B* **1986**, *34*, 2439.
(9) von Barth,U.; Hedin, L. *J. Phys. C* **1972**, *5*, 1629.
(10) Koelling, D.; Harmon, B. N. *J. Phys. C* **1977**, *10*, 3107.
(11) Jepsen, O.; Andersen, O. K. *Z. Phys. B* **1995**, *97*, 645.
(12) Dronskowski, R.; Blöchl, P. E. *J. Phys. Chem.* **1993**, *97*, 8617.
(13) Barrett, C.; Massalski, T. B. *Structure of Metals 3rd revised edition: Crystallographic Methods, Principles, and Data*; International Series on Materials Science and Technology 35; Pergamon Press: Oxford, New York, 1987.

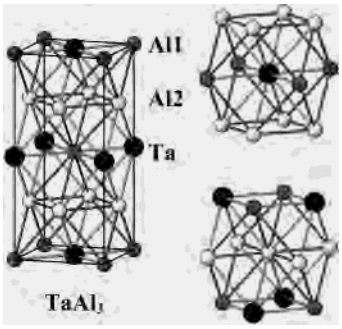

Figure 1. Crystallographic unit cell of $TaAl_3$. Dark circles are Ta; shaded circles are Al1; light circles are Al2 sites. The coordination environments for each site are also highlighted.

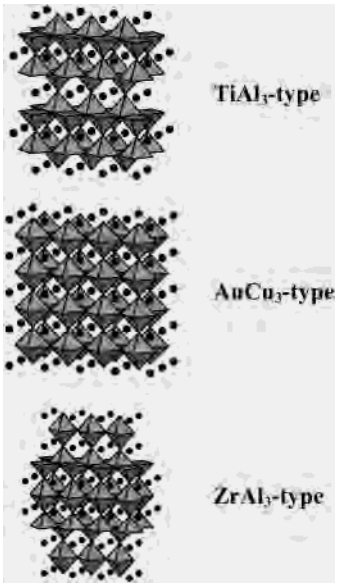

Figure 2. Representation of the three binary AB_3 colorings of the fcc arrangement to emphasize the polyhedra of B atoms. The black dots indicate the A atom sites. (top) Tetragonal $TiAl_3$ type with just square pyramids; (middle) cubic $AuCu_3$ type with just octahedra; (bottom) tetragonal $ZrAl_3$ type with both polyhedra.

Table 3. Anisotropic Displacement Parameters for $TaAl_3$

atom	U_{11}	U_{22}	U_{33}	U_{23}	U_{13}	U_{12}
Ta	0.003 39 (23)	0.003 39 (23)	0.002 60 (24)	0	0	0
Al1	0.004 20 (76)	0.004 20 (76)	0.007 92 (117)	0	0	0
Al2	0.004 99 (56)	0.004 99 (56)	0.003 11 (79)	0	0	0

Table 4. Selected Interatomic Distances (angstroms) for $TaAl_3$

Ta−Al1 (4×)	2.7161 (4)
Ta−Al2 (8×)	2.8718 (4)
Al1−Al2 (8×)	2.8718 (4)
Al2−Al2 (4×)	2.7161 (4)

structure and highlights the coordination environments for the atoms of the asymmetric unit.

The structure of $TaAl_3$ alternates $^{\infty}_{2}$[TaAl] and $^{\infty}_{2}$[AlAl] planar square nets, related by displacement along (1/2)*a*, along the *c* direction with a shift of (1/2)*a* + (1/2)*b* for every pair. In this way, the body-centered tetragonal unit cell is created. From a different viewpoint, the arrangement of Ta atoms creates a network of Al atoms that consists of vertex- and edge-sharing square pyramids, which is highlighted in Figure 2. The remainder of this figure illustrates how this description provides a structural chemical distinction between

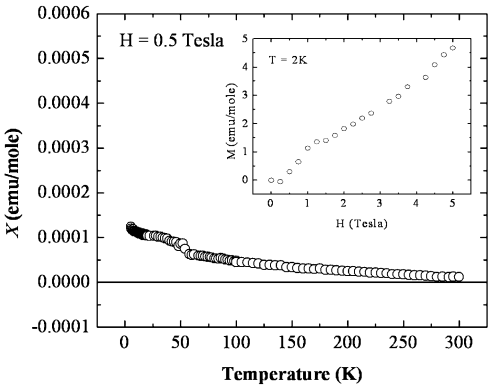

Figure 3. Temperature-dependent susceptibility (0.5 T) and magnetization isotherm (inset, 2 K) of $TaAl_3$.

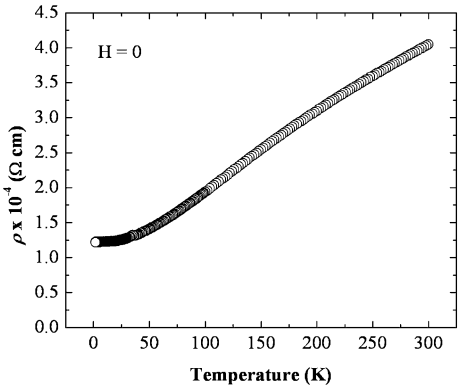

Figure 4. Temperature-dependent, zero-field resistivity of $TaAl_3$.

the structure of $TaAl_3$ and the related structures of the cubic $AuCu_3$ (Strukturbericht designation $L1_2$[13]) and tetragonal $ZrAl_3$ types (Strukturbericht designation $D0_{23}$[13]). Among trialuminides, $LuAl_3$ adopts the cubic $AuCu_3$ type, while the tetragonal $ZrAl_3$ type is the high-temperature form for $HfAl_3$. In $LuAl_3$ the Al network involves octahedra sharing vertexes in all three directions. The tetragonal $ZrAl_3$ may be described as a 1:1 intergrowth structure of the cubic $AuCu_3$ type and tetragonal $TiAl_3$ type with respect to the (001) planes of atoms.

An important feature of the $TaAl_3$ structure is that the *c*/*a* ratio exceeds 2.0, which is the ideal value if the face-centered atomic arrangement remained. The elongation of the *c* axis with respect to the *a* and *b* axes causes shorter Ta−Al and Al−Al distances in the *ab* plane than along the *c* direction.

Physical Properties. The temperature-dependent magnetic susceptibility for $TaAl_3$ at 0.5 T is shown in Figure 3. The inset shows a plot of magnetization verses field at 2 K. The overall behavior of the field-dependent magnetization at 2 K is paramagnetic. The 0.5 T susceptibility measurement exhibits Pauli-like paramagnetic behavior with slight temperature dependence. The feature near 50 K is associated with the so-called "oxygen peak" common for Quantum Design magnetometers in the case of very small signals, and is not intrinsic to the $TaAl_3$ sample.

Temperature-dependent zero-field resistivity curves for $TaAl_3$ are shown in Figure 4. Figure 5 shows a plot of field-dependent resistivity at $T = 2$ K. The inset shows a plot of $\ln(\rho - \rho_o)$ vs $\ln H$ between 5 and 9 T, where ρ_o is the

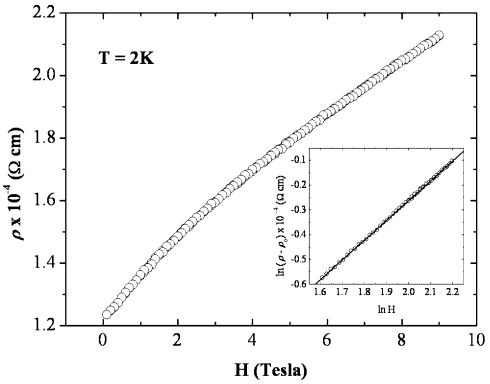

Figure 5. Resistivity versus field of $TaAl_3$. The inset shows a plot of $\ln(\rho - \rho_o)$ versus ln H between 5 and 9 T.

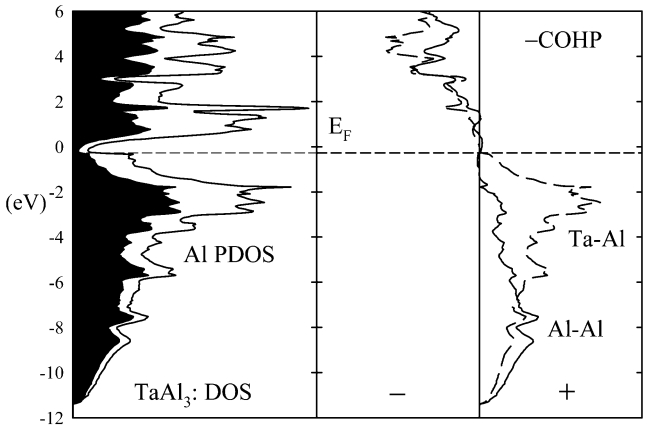

Figure 6. Total density of states (TDOS) and Al PDOS of $TaAl_3$ with the −COHP curves for Al−Al (solid) and Ta−Al (dashed) interactions. The Fermi level is indicated by the dashed line.

resistivity at zero field. The resistivity has expected metallic character with the residual resistance ratio RRR = R(300 K)/R(2 K) equal to 3.3. The resistivity of $TaAl_3$ increases by approximately 70−75% in an applied field of 9 T, and follows the power law $\rho - \rho_o = H^\alpha$, where $\alpha = 0.79$, which was extracted from the equation $\ln(\rho - \rho_o) = \alpha \ln H$. This functional behavior differs drastically from $\rho - \rho_o = H^2$ that is expected and seen in a number of simple metals[14] and, together with the rather large magnetoresistance, may deserve detailed investigation.

Calculated Electronic Structure. The calculated density of states (DOS) with the projection of Al valence orbitals is shown in Figure 6. The Fermi level, indicated by the dashed line, falls near a deep minimum in the DOS curve. This low density of states at the Fermi level is consistent with the small magnetic susceptibility as well as the results of a recent NMR study on $TaAl_3$.[15] Analysis of the orbital interactions via the crystal orbital Hamilton population (COHP) indicates that both the Al−Al bonding and Ta−Al bonding are optimized. Levels near the Fermi level show Al−Al nonbonding character, while the Ta−Al bonding sharply changes from bonding to antibonding and seems to be the most influential in controlling this structure.

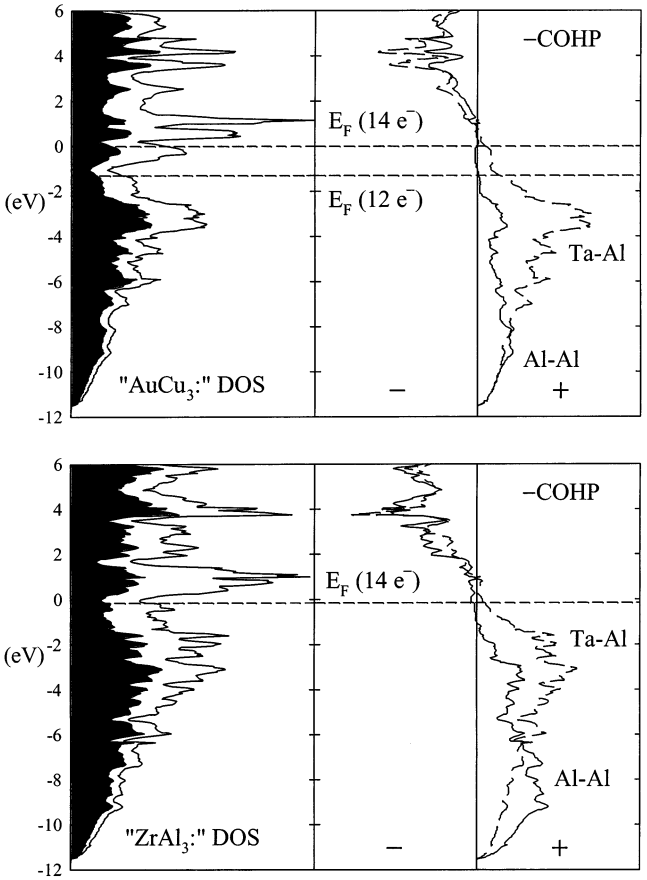

Figure 7. (top) Total density of states (TDOS) and Al PDOS of $TaAl_3$ in the cubic $AuCu_3$ type with the −COHP curves for Al−Al (solid) and Ta−Al (dashed) interactions. The Fermi levels for 14 and 12 electrons are indicated by the dashed line. (bottom) Total density of states (TDOS) and Al PDOS of $TaAl_3$ in the tetragonal $ZrAl_3$ type with the −COHP curves for Al−Al (solid) and Ta−Al (dashed) interactions. The Fermi level for 14 electrons is indicated by the dashed line.

In Figure 7, the DOS and −COHP curves for $TaAl_3$ in the $AuCu_3$-type and $ZrAl_3$-type structures are shown. Clearly, the DOS and −COHP curves resemble those for the observed structure (see Figure 6), but the corresponding Fermi levels do not fall at minima in these DOS curves. Table 5 summarizes the results of computations on the three structure types. We present results for $TaAl_3$ in its actual structure ($c/a = 2.22$) and for an idealized model at the same unit cell volume but where $c/a = 2$. It is noteworthy that the calculated COHP values for the inequivalent Ta−Al and Al−Al bonds in the idealized model structure agree with the observed distortion—the COHP values for bonds in the *ab* plane are more negative (larger) than for those bonds with components along the *c* direction. These COHP values suggest stronger orbital interactions in the *ab* plane, which leads to shorter distances than those along the *c* axis. The results in Table 5 and Figure 7 also confirm the earlier calculations reported by Freeman and co-workers that the stability of these trialuminides follow a rigid-band argument.

In the $D0_{22}$ structure type of $TaAl_3$, there are two inequivalent crystallographic sites for Al atoms. These are highlighted in Figure 1 by the shaded and unshaded Al sites. According to Table 5, the Al1 site (surrounded by a square planar arrangement of Ta atoms; shaded in Figure 1)

(14) Pippard, A. B. *Magnetoresistance in Metals*; Cambridge University Press: Cambridge, UK, 1989.
(15) Lue, C.-S.; Chepin, S.; Chepin, J.; Ross, J. H., Jr. *Phys. Rev. B* **1998**, *57*, 7010−7014.

Table 5. Results from TB-LMTO-ASA Calculations on $TaAl_3$ and Various fcc-Type Models

	obsd structure	ideal $TiAl_3$ type	$AuCu_3$ type	$ZrAl_3$ type
total energy (eV)	0	+0.341	+0.695	+0.497
Fermi energy (eV)	−0.278	−0.389	−0.008	−0.138
Q_{Ta} (e^-)				
s	0.623	0.708	0.712	0.705
p	0.738	0.815	0.748	0.782
d	3.603	3.674	3.655	3.667

	obsd structure		ideal $TiAl_3$ type			$ZrAl_3$ type	
	Al1	Al2	Al1	Al2	$AuCu_3$ type	Al1	Al2
Q_{Al} (e^-)							
s	1.043	1.036	1.063	1.004	1.017	1.048	1.008
p	1.659	1.352	1.399	1.555	1.523	1.403	1.534
d	0.426	0.318	0.366	0.381	0.383	0.394	0.386

	obsd structure	ideal $TiAl_3$ type	$AuCu_3$ type
COHP (eV)			
Al−Al	−0.030; −0.056	−0.060; −0.072	−0.067
Ta−Al	−0.134; −0.104	−0.117; −0.116	−0.111

accumulates a lower valence electron density than the Al2 sites. Therefore, novel ternary compounds could be targeted with this structure that could lead to interesting properties for intermetallic compounds, e.g., semiconductivity[16] or half-metallic ferromagnetism.[17] For example, the Al2 sites would be more energetically attractive for electronegative metal atoms such as Ga—preliminary electronic structure calculations on a hypothetical "$TaAlGa_2$" indicate an energy gap at the Fermi level. Furthermore, earlier electronic structure calculations on Fe- or Zn-doped $TiAl_3$ and $NbAl_3$ did show enhanced stability of the cubic $L1_2$ structure, but did not address the atomic arrangements.[18] Synthetic efforts to prepare novel ternary analogues of these structures are currently underway.

The network description of these structures begs the use of a Wade's rule argument to understand these structures. Vajenine and Hoffmann have elucidated "magic electron counts" for networks of vertex-sharing aluminum octahedra using extended Hückel theory.[19] According to Wade,[20] an isolated octahedral cluster of main group elements requires 26 valence electrons: 12 belong to the six lone pair orbitals directed radially away from the cluster center; 14 belong to seven skeletal bonding orbitals, which may be divided into two electrons in one bonding radial orbital and 12 electrons in six bonding tangential orbitals. In the cubic $AuCu_3$-type structure observed for $LuAl_3$, there is a three-dimensional (3D) network of vertex-sharing octahedra. Vajenine and Hoffmann demonstrated via the band structure and an overlap population analysis by taking into account first and second nearest neighbor Al−Al interactions that eight valence skeletal electrons are required for the cubic Al network in the structure of $LuAl_3$.

(16) (a) Häussermann, U.; Boström, M.; Viklund, P.; Rapp, Ö.; Björnängen, T. *J. Solid State Chem.* **2002**, *165*, 94. (b) Springborg, M.; Fischer, R.; Rudiger, *J. Phys.: Condens. Matter* **1998**, *10*, 701.
(17) de Groot, R. A.; Buschow, K. H. J. *J. Magn. Magn. Mater.* **1986**, *54*−*57*, 1377.
(18) Carlsson, A. E.; Meschter, P. J. *J. Mater. Res.* **1990**, *5*, 2813−2818.
(19) Vajenine, G. V.; Hoffmann, R. *J. Am. Chem. Soc.* **1998**, *120*, 4200.
(20) Wade, K. *Adv. Inorg. Chem. Radiochem.* **1976**, *18*, 1.

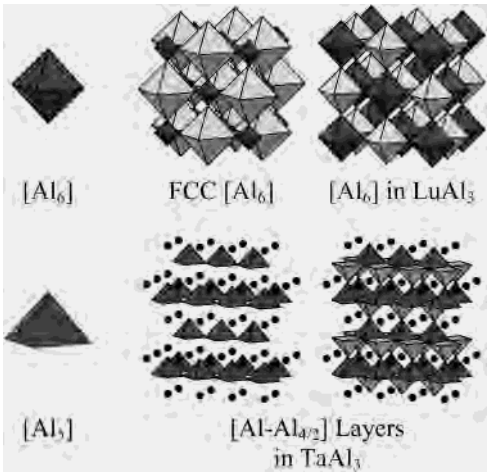

Figure 8. Progression from the isolated $[Al_6]$ octahedron through the fcc arrangement of $[Al_6]$ octahedra to the Al network in $LuAl_3$. The lightly shaded octahedra represent the clusters generated by bringing together several isolated clusters. The electron counting scheme for this progression is described in ref 19.

There is another, simpler way to reach this value (see Figure 8): the cubic network of vertex-sharing octahedra can be created by bringing $[Al_6]$ octahedra together into a fcc array. This arrangement creates larger octahedra between the clusters. When the unit cell edge equals 2×2 times the Al−Al distance in a cluster, the sizes of the two octahedra are identical and the 3D cubic network found in $LuAl_3$ occurs. Upon forming the fcc array, six lone pair orbitals will create six skeletal radial orbitals in the newly forming octahedra—only one of these (the a_{1g} combination) will create a bonding orbital. Therefore, as the fcc network forms, the two octahedral units have 14 and 2 skeletal bonding electrons. When the two octahedra achieve equal sizes, then there can be no more than 16 skeletal bonding electrons distributed among the two clusters. That is, there will be eight skeletal bonding electrons per octahedra. Vajenine and Hoffmann also showed that the number of skeletal electrons per cluster that is optimal for Al−Al bonding in a two-dimensional sheet of vertex-sharing octahedra is 10. Again, as seen in Figure 8, the network of square pyramids in $TaAl_3$ involves layers of vertex-sharing square pyramids. Since the octahedron and square pyramid require the same number of skeletal bonding electrons, we conclude that by nature of the construction of this structure, 10 skeletal electrons per formula unit optimizes Al−Al bonding. This is borne out in the overlap population curve for this structure.

As a final point, we will address the orbital interactions between the metal atom and the Al network in the two alternatives: the $AuCu_3$ type and the $TiAl_3$ type. The site symmetry for the metal atom in each structure is, respectively, O_h and D_{4h} and the coordination environment is a cuboctahedron. In the cubic structure, the valence d orbitals will split into e_g and t_{2g} sets of orbitals. At the Γ point, the e_g orbitals are stabilized by mixing with a cluster e_g orbital from the Al 3s orbitals; the t_{2g} orbitals remain completely nonbonding. At the R point, the e_g orbitals are stabilized by mixing with a cluster e_g orbital from the Al 3p orbitals; the t_{2g} orbitals are destabilized by mixing with a cluster bonding t_{2g} orbital from the Al 3p orbitals. Throughout the band

structure, the metal e_g orbitals lie among the occupied orbitals through M−Al bonding overlap. In the tetragonal structure, the d orbitals split in a similar fashion because the coordination polyhedra is nearly cuboctahedral, and the "e_g-like" orbitals also lie among the occupied orbitals. Therefore, the cubic $AuCu_3$ structure for MAl_3 achieves optimum bonding for 12 valence electrons (eight electrons for the Al network + four electrons in the M e_g orbitals), whereas the tetragonal $TiAl_3$ structure achieves optimum bonding for 14 valence electrons (10 electrons for the Al network + 4 electrons in the M "e_g" orbitals). Further investigations of the electronic structures of various other 3D networks of main group polyhedra are underway.

Conclusions

$TaAl_3$ grows in an Al flux and provides optimal samples for single-crystal X-ray diffraction at ca. 2 at. % Ta in Al. The crystal structure adopts the tetragonal $TiAl_3$ structure type ($D0_{22}$ type) with two distinct sites for Al atoms. These two sites allow targeting possible new ternary (pseudobinary) intermetallic compounds that may show semiconducting behavior for a close-packed structure. Finally, the structures of $TaAl_3$ and related covalent trialuminides can be described using modification of Wade's rules.

Acknowledgment. This work was supported by the National Science Foundation through Grants DMR 9981766 and 36481AC5. Ames Laboratory is operated for the U.S. Department of Energy by Iowa State University under Contract No. W-7405-Eng.-82. Work at the Ames Laboratory was supported by the Director for Energy Research, Office of Basic Energy Sciences.

Supporting Information Available: Crysallographic data in CIF format. This material is available free of charge via the Internet at http://pubs.acs.org.

IC034927M